

Unraveling of a Tethered Polymer Chain in Uniform Solvent Flow

Aruna Mohan and Patrick S. Doyle*

Department of Chemical Engineering, Massachusetts Institute of Technology,
Cambridge, Massachusetts 02139

Received January 8, 2007; Revised Manuscript Received March 20, 2007

ABSTRACT: The separation of electrophoresing DNA molecules of varying lengths, actuated by their size-dependent collision with a stationary obstacle or array of obstacles, has recently gained prominence. To gain insight into how a chain initially unravels subsequent to a polymer–obstacle collision, we investigate the stretching dynamics of a tethered polymer chain initially at equilibrium, following the imposition of a uniform flow of solvent. The solution for the Rouse model of the polymer chain is obtained via an analysis into normal modes. We examine the consequences of finite chain extensibility by performing Brownian dynamics simulations of the wormlike chain model, which describes DNA elasticity. Detailed results are presented for the propagation of tension with time in Rouse and wormlike chains. Our results suggest the diffusive propagation of tension in Rouse chains, whereas a convective mechanism of tension propagation in wormlike chains under conditions of strong flow is demonstrated.

1. Introduction

Recently, a size-based method for the separation of DNA chains of varying lengths has emerged, based on the electrophoresis of the DNA chains through an array of obstacles. The size specificity of this separation technique arises from the fact that a longer chain, upon its collision with an obstacle, requires more time for disentanglement than a shorter chain. Such a separation technique was pioneered by Volkmuth and Austin,¹ who employed optical microlithography to fabricate obstacle courses in silicon dioxide. More recently, as described in a series of papers, Randall and Doyle^{2–4} have used soft lithography to construct PDMS microchannels enclosing an obstacle or array of obstacles and have investigated chain dynamics following polymer–obstacle collisions. In the experiments of Doyle et al.⁵ and subsequently Minc et al.,⁶ the obstacle course was instead formed from a suspension of superparamagnetic particles, which self-assembled into a quasi-regular array of columns upon the application of a magnetic field. Size-based separation has also been achieved via dilute solution capillary electrophoresis, wherein a dilute solution of neutral polymer chains is used as the separation medium.^{7,8} The separation is induced by the size-dependent entanglement of the DNA molecules with the neutral host polymer chains.^{9,10} These, as well as related studies on the electrophoretic separation of DNA molecules, are discussed in the review of Viovy.¹¹

The transient unraveling of the polymer chain following a polymer–obstacle collision and the formation of a hooked configuration is a feature common to the above-mentioned size-based separation techniques. The dynamics of DNA molecules in an array of obstacles have been modeled by Minc et al.¹² and Dorfman¹³ as a continuous time random walk comprising three distinct stages, namely, collision with a post and the unraveling of the two arms, unhooking from the post, and finally unhindered electrophoretic motion until the next collision. An improved understanding of the dynamics following impact is expected to refine predictions of the unraveling and unhooking times, and, ultimately, the separation resolution attainable in these devices.

In this direction, several models of polymer–obstacle hooking aimed at deducing the unhooking time following a collision were proposed by Randall and Doyle.⁴ In particular, the “X model” is proposed for collisions occurring under strong electric fields or, equivalently, at high Peclet numbers. The validity of the X model is restricted to situations wherein the long arm of the chain continues to unravel as the chain is unhooking from the post. The model hypothesizes that the long arm can be decomposed into a tension-bearing section terminated by a freely convected coil, convected at the free solution electrophoretic velocity. It is further assumed that the length of the tension-bearing portion of the long arm increases at a rate equal to the electrophoretic velocity as the freely convected coil unwinds. One of the objectives of the present investigation is to test this assumption of convective tension propagation in a chain unraveling in an external field.

Under the assumption that the unraveling and unhooking events are decoupled, the unraveling of each arm of the chain following its collision with an obstacle may be modeled as being equivalent to the stretching of a chain tethered to the obstacle under an imposed field. The X model, in assuming that the tension propagation in the long arm is significantly faster than the ropelike unhooking motion of the chain, also allows for such a decoupling.⁴ Finally, we invoke the principle of electrohydrodynamic equivalence,^{14,15} which states that chain stretching in an electric field is equivalent to that in a uniform hydrodynamic flow field at a flow velocity equal to the free solution electrophoretic velocity of the chain. Such an equivalence holds especially under the free draining conditions assumed in the present study, justified partially by the screening of hydrodynamic interactions in complicated channel geometries. However, more generally, hydrodynamic interactions arising on average from the electric-field-induced motion of individual polymer segments are screened by the counterion cloud surrounding the polyelectrolytic DNA molecule over distances exceeding the Debye length.¹⁴ With the above assumptions, a parallel between the stretching of a tethered chain in an electric field and that in a hydrodynamic flow field may be established.

Several studies exist on the steady-state properties of a tethered chain in uniform flow. The stretching of a tethered DNA

* Corresponding author. E-mail: pdoyle@mit.edu.

molecule in uniform flow was experimentally visualized and the dependence of steady fractional extension on velocity and chain length obtained by Perkins et al.¹⁶ Larson et al.¹⁷ performed Monte Carlo simulations of DNA chains used in the experiments of Perkins et al. as well as of longer chains, whereas Cheon et al.¹⁸ employed molecular dynamics simulations of chains of several lengths. These studies concentrated on the steady-state behavior of chain extension. Scaling arguments were proposed for the steady extension of a chain modeled as a string of nondraining blobs in uniform flow by Brochard-Wyart,^{19,20} based on the trumpet picture for moderate stretching and the stem-and-flower picture for strong stretching. Several static properties of a tethered chain in a uniform flow field, including end-to-end distance, drag, and tension distribution, have been investigated by Zimmermann and co-workers,^{21,22} using the bead–spring model both with and without account for excluded volume and hydrodynamic interactions and analytical calculations based on the equilibrium configurational distribution or the blob model. These authors employ the Gaussian, FENE, and freely jointed chain models.

The dynamics of stretching, however, remain relatively unexplored. Scaling arguments have been proposed by Brochard-Wyart and co-workers^{20,23} for the transient extension of a tethered chain stretched by the application of a constant force at the free end or by a flow field in the trumpet regime and for stretching in a flow field and relaxation upon cessation of flow in the stem-and-flower regime. Existing simulation studies of chain dynamics in uniform flow are restricted to the near-equilibrium or near-steady-state regimes. Avramova et al. provide a Monte Carlo study of the near-equilibrium stretching of a chain upon the imposition of flow and its relaxation following the cessation of flow.²⁴ Conformational fluctuations of tethered Rouse and FENE chains in flow at steady state have been studied in detail by Rzehak and Zimmermann^{25,26} and Rzehak.²⁷ A few recent studies have theoretically treated tension propagation in stiff polymers under external fields²⁸ and in semiflexible polymers under the application of a pulling force.²⁹ However, a description of the transient stretching of a semiflexible, wormlike chain in flow is lacking.

The aim of the present investigation is to provide a comprehensive study of chain unraveling in uniform flow. The Rouse model is selected for its analytical tractability. The consequences of finite extensibility are examined via Brownian dynamics simulations of DNA chains described by the wormlike chain model, in the absence of other nonlinear effects such as excluded volume and hydrodynamic interactions. The paper is organized as follows. In section 2, we describe the problem under consideration and the methods of analysis adopted. Analytical results for the Rouse model are presented in section 3. Section 4 provides a comparison between the behavior of Rouse and wormlike chains and describes the scaling behavior of the latter model. Results for tension propagation in Rouse and wormlike chains are presented in section 5. Section 6 contains a summary of our findings.

2. Problem Definition and Methodology

In this study, we employ the bead–spring model of the polymer chain, whereby the chain is discretized into N beads, indexed from 0 to $N - 1$, with each pair of adjacent beads connected by a spring. The first bead of the chain is held tethered. The chain is initially in an equilibrium, coiled configuration, and at time $t = 0$, a uniform flow of solvent is imposed, with $\mathbf{v} = v\hat{\mathbf{x}}$ denoting the unperturbed solvent velocity and $\hat{\mathbf{x}}$ the unit vector in the flow direction. Under the free

draining assumption, the set of Langevin equations governing the evolution of the chain is

$$d\mathbf{r}_0 = 0 \quad (1)$$

$$d\mathbf{r}_j = \left(\mathbf{v} + \frac{1}{\zeta} \mathbf{F}_j \right) dt + \sqrt{\frac{2k_B T}{\zeta}} d\mathbf{W}_j, \quad j = 1, \dots, N - 1 \quad (2)$$

where \mathbf{r}_i , $i = 0, \dots, N - 1$, denotes the position vector of bead i relative to the origin, chosen here to lie at the location of the tethered bead ($\mathbf{r}_0 = \mathbf{0}$), and \mathbf{F}_j refers to the net deterministic force acting on bead j . In the absence of excluded volume interactions and external forces, the latter is identical to the spring force exerted on bead j by the adjoining springs. The drag coefficient for a single bead, given by Stokes' law, is denoted by ζ , and $k_B T$ denotes the thermal energy. The term \mathbf{W}_j represents a three-dimensional Wiener process, with $\langle d\mathbf{W}_j(t) \rangle = \mathbf{0}$ and $\langle d\mathbf{W}_j(t) d\mathbf{W}_k(t') \rangle = dt \delta_{jk} \delta(t - t') \boldsymbol{\delta}$, where $k = 1, \dots, N - 1$ and $\boldsymbol{\delta}$ is the identity tensor.

We consider DNA molecules of five lengths, namely, λ -DNA (having a contour length of 21 μm when stained with YOYO dye in the ratio of 4 base pairs of DNA per molecule of dye), 2λ -DNA, 4λ -DNA, 6λ -DNA, and 10λ -DNA. The persistence length of DNA, assumed unchanged on staining, is known to be 53 nm. We maintain a constant level of discretization in our study and vary the number of beads N in the bead–spring model to accommodate chains of different lengths. As a compromise between achieving satisfactory resolution of the chain into springs while concurrently ensuring an acceptable computational speed, we select a discretization of $N_{k,s} = 19.8$ Kuhn lengths per spring, with the Kuhn length b_k being equivalent to two persistence lengths, i.e., $b_k = 0.106 \mu\text{m}$.

The elasticity of DNA is characterized by the wormlike chain model, the force–extension behavior of which is commonly described by an interpolation formula due to Marko and Siggia.³⁰ However, Underhill and Doyle³¹ have noticed that errors result from the formulation of a bead–spring model with the use of the Marko–Siggia interpolation formula (which describes the global force–extension behavior of the polymer molecule stretched at constant force) to determine the force–extension behavior of each spring. These errors may be compensated in part by replacing the true persistence length with an effective persistence length in the Marko–Siggia force law. We adopt the ratio $\lambda = 1.1$ of the effective persistence length to the true persistence length, found by Underhill and Doyle to eliminate errors at 50% mean fractional chain extension. The resulting force law is

$$\mathbf{F}_{\text{spr}}(\mathbf{Q}) = \frac{k_B T}{2\lambda b_k} \left[\left(1 - \frac{Q}{Q_0} \right)^{-2} - 1 + 4 \frac{Q}{Q_0} \right] \frac{\mathbf{Q}}{Q} \quad (3)$$

where \mathbf{F}_{spr} denotes the spring tension, \mathbf{Q} the spring vector of magnitude Q , and $Q_0 = N_{k,s} b_k$ the maximum spring length. Consequently, the contour length L is equal to $(N - 1)Q_0$. In the linear regime corresponding to $Q \ll Q_0$, the Marko–Siggia force law reduces to Hooke's law with a spring constant of $H = 3k_B T / (\lambda b_k^2 N_{k,s})$, employed in our solution of the Rouse model.

We characterize the strength of the solvent flow by means of a Peclet number, defined as $\text{Pe} = vN\zeta / (k_B T / b_k)$, physically equivalent to the dimensionless drag force acting on a chain of N beads. The diffusivity underlying our definition of Pe is, therefore, that of an unconstrained, free draining chain of N beads as given by $D = k_B T / (N\zeta)$. (However, in the limit of large N , the difference between the use of N or $N - 1$ in the definition of the Peclet number and elsewhere is immaterial. Such

differences will be ignored throughout this study.) This definition of the Peclet number is motivated by the observation that the fractional chain extension at steady state is a universal function of the drag force acting on the chain, regardless of chain length.^{16,17,21} Furthermore, steady-state results for a tethered freely jointed chain are known to reduce to the corresponding results for a Gaussian chain in situations wherein $Pe \ll 1$.²¹ Therefore, we may expect a crossover from the linear, near-equilibrium regime to a regime of strong chain stretching dominated by finite extensibility at a Peclet number of the order of 1. In the present investigation, we consider a range of Peclet numbers from 1 to 100. Assuming a temperature of 298 K, a Peclet number of 100 corresponds to a drag force of 4 pN on a DNA chain, which falls significantly below the value of 65 pN at which the stretching phase transition occurs. The Marko–Siggia law remains valid for DNA molecules stretched to an extension of up to 97% or up to a Peclet number of $Pe = 600$.³⁰

Equations 1 and 2, with the spring force law given by Hooke's law in the Rouse model, reduce to a linear set of Langevin equations and are amenable to an analysis into normal modes. The wormlike chain model is treated via Brownian dynamics simulations. Initial equilibrium configurations are generated by employing the Marko–Siggia force law to simulate the evolution to equilibrium of Gaussian coils. The radius of gyration of an initially Gaussian configuration converges to its steady, equilibrium value within 5 relaxation times for all the simulated chain lengths, and the resulting configuration is subsequently sampled at intervals of 1 relaxation time to obtain starting configurations for our simulations. We adopt the semiimplicit predictor–corrector scheme described in ref 32 for the integration of eq 2. A time step of $5 \times 10^{-4} \zeta Q_0^2 / (k_B T)$ is used. The equilibrium radius of gyration and chain stretch of λ -DNA in the absence of flow were found to vary by less than 2% upon reducing the time step by a factor of 5. Averages are performed over an ensemble of 100 chains. Upon doubling the ensemble size to 200 chains, the equilibrium radius of gyration and chain stretch were found to differ by less than 1% from the corresponding values obtained from an ensemble of 100 chains for λ -DNA in the absence of flow, with thermal noise being further attenuated in the presence of flow. However, in order to facilitate an accurate determination of the instantaneous chain length under tension in flow, the results presented for a 61-bead wormlike chain at $Pe = 10$ and $Pe = 30$ derive from ensemble sizes of 10 000 and 1000, respectively.

Except where dimensional notation proves convenient, non-dimensional variables will be employed in the remainder of this study and will be denoted by the symbol “ \sim ” surmounting the corresponding dimensional variable. We utilize a length scale of Q_0 and a time scale of $\zeta Q_0^2 / (k_B T)$. Consequently, the unit of force employed by us is $k_B T / Q_0$, with the spring constant expressed in units of $k_B T / Q_0^2$.

3. The Rouse Model

Below, we summarize our results for the end-to-end distance and the tension distribution in a Rouse chain and highlight their relevant features. The details of the normal mode solution are relegated to the Appendix. We obtain

$$\tilde{L}_e = \frac{Pe}{\tilde{H}} \frac{N_{k,s}}{N} \sum_{m,j=1}^{N-1} \Omega_{N-1,m} \Omega_{jm} \frac{1 - \exp(-\tilde{H} a_m \tilde{t})}{a_m} \quad (4)$$

$$\tilde{F}_{\text{spr } 1, x} = Pe \frac{N_{k,s}}{N} \sum_{m,j=1}^{N-1} \Omega_{1m} \Omega_{jm} \frac{1 - \exp(-\tilde{H} a_m \tilde{t})}{a_m} \quad (5)$$

and

$$\tilde{F}_{\text{spr } k, x} = Pe \frac{N_{k,s}}{N} \sum_{m,j=1}^{N-1} (\Omega_{km} - \Omega_{k-1,m}) \Omega_{jm} \frac{1 - \exp(-\tilde{H} a_m \tilde{t})}{a_m} \quad k = 2, \dots, N-1 \quad (6)$$

where \tilde{L}_e and $\tilde{F}_{\text{spr } k, x}$ denote respectively the mean end-to-end distance and spring tension in spring k in the flow direction, with the index $k = 1, \dots, N-1$ measured from the tethered end. The end-to-end distance is measured by the x -coordinate of the bead at the free end of the chain. The elements of the matrix Ω , composed of the normalized eigenvectors of the Rouse matrix, are given by²⁶

$$\Omega_{jm} = \frac{1}{\sqrt{\frac{N}{2} - \frac{1}{4}}} \sin\left(\frac{2m-1}{2N-1} \pi j\right) \quad (7)$$

corresponding to the eigenvalues

$$a_m = 4 \sin^2\left(\frac{2m-1}{2N-1} \frac{\pi}{2}\right) \quad (8)$$

It is evident from eqs 4–8 that the relaxation times of a tethered Rouse chain may be identified with

$$\tilde{\tau}_m = \frac{1}{\tilde{H} a_m} \quad (9)$$

Equations 4–6 may be simplified by means of elementary trigonometric identities, and the summations $\sum_j \Omega_{jm}$ and the term $\Omega_{N-1,m}$ approximated in the limit of large N , yielding

$$\tilde{L}_e = \frac{Pe}{\tilde{H}} \frac{N_{k,s}}{4N^2} \sum_{m=1}^{N-1} (-1)^{m+1} \frac{1 - \exp(-\tilde{t}/\tilde{\tau}_m)}{\sin^3\left(\frac{2m-1}{2N-1} \frac{\pi}{2}\right)} \quad (10)$$

and

$$\tilde{F}_{\text{spr } k, x} = Pe \frac{N_{k,s}}{2N^2} \sum_{m=1}^{N-1} \cos\left(\frac{2m-1}{2N-1} (2k-1) \frac{\pi}{2}\right) \frac{1 - \exp(-\tilde{t}/\tilde{\tau}_m)}{\sin^2\left(\frac{2m-1}{2N-1} \frac{\pi}{2}\right)} \quad k = 1, \dots, N-1 \quad (11)$$

The scaling behavior of Rouse chains is manifest in eqs 10 and 11. Owing to the linearity of the Rouse model, the dependence on Pe is trivial. The behavior of the chain extension and tension distribution as N is varied may be gauged from the fact that the slow modes dominate the dynamics, except very close to $\tilde{t} = 0$. This is true particularly as the dependence on a_m , which rapidly increases with m , approaching a value of 4 as m approaches $N-1$, arises not only in the decaying exponent but also in the form of inverse powers of a_m in eqs 10 and 11. Similar to the case of an unconstrained Rouse chain, $a_m \sim 1/N^2$ and, consequently, $\tau_m \propto N^2$ for the slow modes ($m \ll N$) and for long chains ($N \gg 1$). It then follows that the chain extension expressed as a fraction of the contour length, namely, \tilde{L}_e/N , and the tension in the first spring, $\tilde{F}_{\text{spr } 1, x}$, which balances the drag acting on the chain at steady state and is equivalent to the restoring force experienced at the tethered chain end, are universal functions of the rescaled time coordinate \tilde{t}/N^2 at fixed Pe . Similarly, the tension distributions for chains of varying lengths, compared at fixed Pe and at equal values of \tilde{t}/N^2 ,

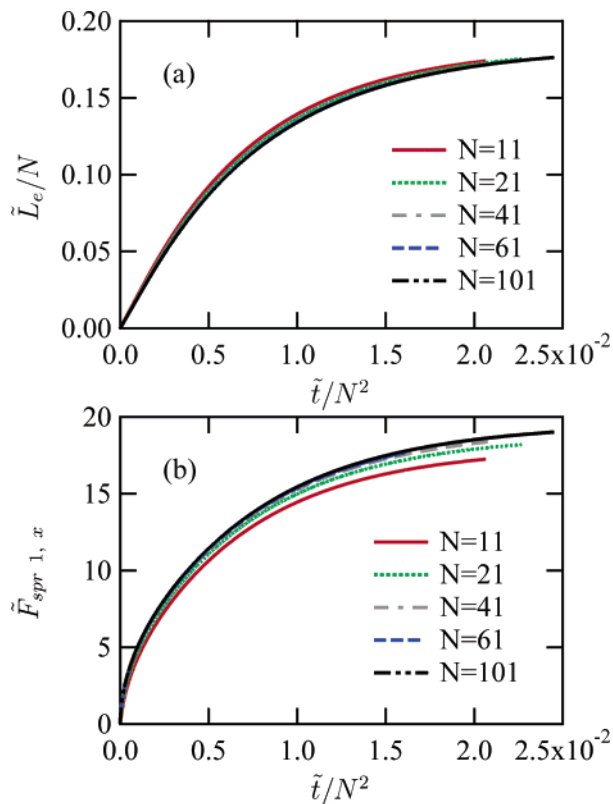


Figure 1. Fractional extension (a) and tension in the first spring (b) as functions of the rescaled time coordinate \tilde{t}/N^2 for Rouse chains of several lengths N at a Peclet number of 1.

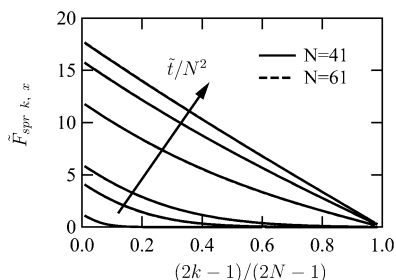


Figure 2. Tension profiles for Rouse chains of 41 and 61 beads as functions of the rescaled spring index $(2k-1)/(2N-1)$ at a Peclet number of 1 at several points in time, compared at $\tilde{t}/N^2 = 6.0 \times 10^{-5}$, 6.7×10^{-4} , 1.3×10^{-3} , 5.4×10^{-3} , 1.1×10^{-2} , and 1.6×10^{-2} for both chain sizes.

collapse when plotted as functions of $(2k-1)/(2N-1)$. This behavior is demonstrated in Figures 1 and 2.

Equation 10 reveals that the contributions from the various modes to the chain extension alternate in sign, with the dominant, positive contribution being that of the slowest mode, $m=1$. As a result, eq 10 may be well-approximated by a single-exponential relaxation to steady state with time constant $\tilde{\tau}_1$, an approximation that marginally overestimates the chain extension (resulting in a maximum error of about 5% for a chain of 61 beads at $Pe=1$). The same approximation predicts the spring tensions with varying degrees of accuracy as k is varied, owing to the fact that the cosine term in eq 11 varies in sign as its argument varies for $k > 1$, resulting in a maximum error of about 20% for the case $k=1$ and $N=61$ at $Pe=1$. Several modes are required to yield accurate tension profiles, with the use of the first 10 modes being found to adequately capture the shape of the transient tension profiles for the case $N=61$.

Equations 4–6 lead to simplified predictions in the short time limit of $\tilde{t} \ll \tilde{\tau}_m$ for all values of m , yielding the convective

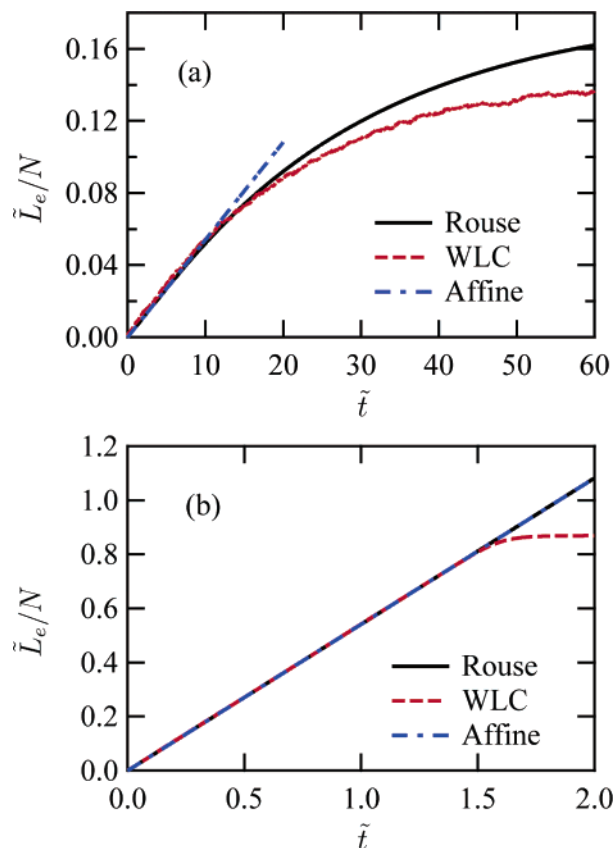


Figure 3. Fractional extension as a function of time for 61-bead Rouse chains and wormlike chains (abbreviated WLC) at Peclet numbers of (a) 1 and (b) 100. Also shown is the fractional extension predicted in the affine deformation limit, namely, $L_e = vt$.

behavior $L_e = vt$ and $F_{spr 1, x} = Hvt$ in dimensional units. An initial region of vanishing tension is predicted for the remaining springs, indexed $k > 1$. The assumption $\tilde{t} \ll \tilde{\tau}_{N-1}$ is, however, valid only in an extremely narrow time window. With $N=61$, we obtain $\tilde{\tau}_{N-1} \approx 5 \times 10^{-3}$, leading to a time interval barely discernible in Figure 1. The chain extension measured by the end-to-end distance does, however, show convective behavior. This behavior arises from the fact that the bead at the free end of the chain is initially convected by the flow, until the preceding spring begins to deform. This issue is discussed further in section 5.

Single-exponential relaxation is predicted by eqs 4–6 in the long time limit of $\tilde{t} \gg \tilde{\tau}_2$, while simultaneously $\tilde{t} \geq \tilde{\tau}_1$. Owing to the existence of almost an order of magnitude difference between the relaxation times of the two slowest modes, the range of validity of this approximation is reasonably large. For instance, for a chain of 61 beads, $\tilde{\tau}_2 \approx 3$, whereas $\tilde{\tau}_1 \approx 28$.

4. The Wormlike Chain Model

The approximation of a wormlike spring by a Gaussian spring is valid for spring extensions below $\sim 30\%$, i.e., under near-equilibrium conditions.³⁰ A comparison between the fractional chain extension and the tension in the first spring predicted by the Rouse and wormlike chain models for $N=61$ at Peclet numbers of 1 and 100 is presented in Figures 3 and 4. The Rouse model is seen to provide a reasonable approximation of a wormlike chain at a Peclet number of 1, but as the Peclet number is increased, deviations from Gaussian behavior are apparent. The seeming agreement between the two models in predicting the chain end-to-end extension, as shown by Figure 3, arises

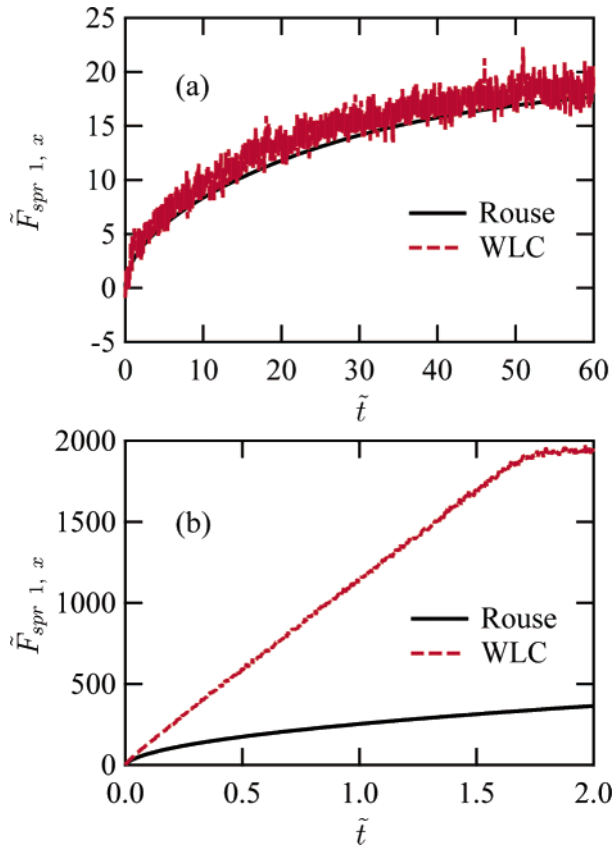


Figure 4. Tension in the first spring as a function of time for 61-bead Rouse and wormlike chains at Peclet numbers of (a) 1 and (b) 100.

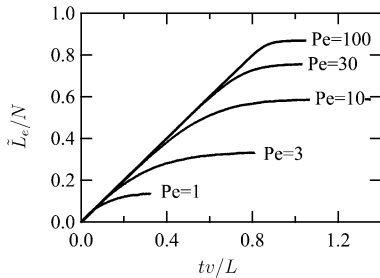


Figure 5. Fractional extension as a function of time nondimensionalized by the convective time scale L/v for a 61-bead wormlike chain at several values of the Peclet number.

due to the convective transport of the free chain end at high Peclet numbers. In particular, at a Peclet number of 100, the affine movement of the chain end of a wormlike chain, leading to the behavior $L_e = vt$, is seen to occur almost until steady state is reached.

Figure 5 shows the evolution of the fractional chain extension as a function of time nondimensionalized by the convective time scale, i.e., tv/L , for a wormlike chain of 61 beads at several flow strengths. The curves initially show affine behavior, corresponding to a line of unit slope passing through the origin. The duration of affine deformation increases with the Peclet number, and in the limit $Pe \rightarrow \infty$, affine deformation is expected to occur until steady state. The steady chain extension of a strongly stretched wormlike chain acted upon by a stretching force f may be estimated from the large force limit of the Marko–Siggia law, given in dimensional form by the expression

$$\frac{fb_k}{k_B T} \approx \frac{1}{2(1 - L_e/L)^2} \quad (12)$$

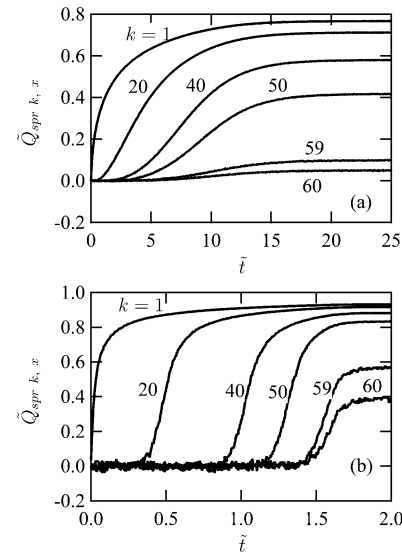


Figure 6. Spring extension in the flow direction, $\tilde{Q}_{\text{spr } k, x}$, plotted against time for several springs of a 61-bead wormlike chain at Peclet numbers of (a) 10 and (b) 100. The label k refers to the spring index measured from the tether point.

With the neglect of the nonuniformity in tension along the chain, f may be replaced by the drag force acting on the chain, $vN\zeta$, to yield

$$1 - \frac{L_e}{L} = (2Pe)^{-1/2} \quad (13)$$

The components of the spring vectors in the flow direction are plotted against time for several springs of a wormlike chain with $N = 61$ at $Pe = 10$ and 100 in Figure 6. At a moderate Peclet number of 10, the simultaneous, nonlinear deformation of several springs contributes to the chain extension once the spring at the free end of the chain, with $k = 60$, begins to deform. On the other hand, at a high Peclet number of 100, spring 60 does not deform almost until steady state is reached. As a result, bead 61 is freely convected, and the chain extension shows affine deformation almost until steady state. The region where nonlinear behavior is manifest in Figure 5 shrinks as Pe is increased.

These features point to the inherent differences between Gaussian and finitely extensible springs. The Gaussian springs close to the tether point of a Rouse chain can continue to extend until steady state. On the other hand, the springs of a wormlike chain close to the tether point, where the drag force exerted by flow is maximum, are quickly stretched close to their steady values, after which they exhibit little deformation. These issues also arise in the qualitatively different nature of tension propagation in Rouse and wormlike chains.

Motivated by the scaling behavior of Rouse chains, we next investigate the collapse of data for wormlike chains of different chain lengths. Figures 7 and 8 demonstrate the collapse of the fractional chain extension and the tension in the first spring, respectively, when plotted as functions of \tilde{t}/N^2 for several chain lengths at three values of the Peclet number. The tension profiles are found to collapse when compared at equal values of \tilde{t}/N^2 for different values of N on replacing the discrete spring index k with a continuous measure of distance along the chain, k/N . This behavior is depicted in Figure 9 at $Pe = 10$ and 100 .

5. Tension Propagation

A strongly stretched wormlike chain exhibits linear tension profiles at all times after an initial period of Gaussian stretching,

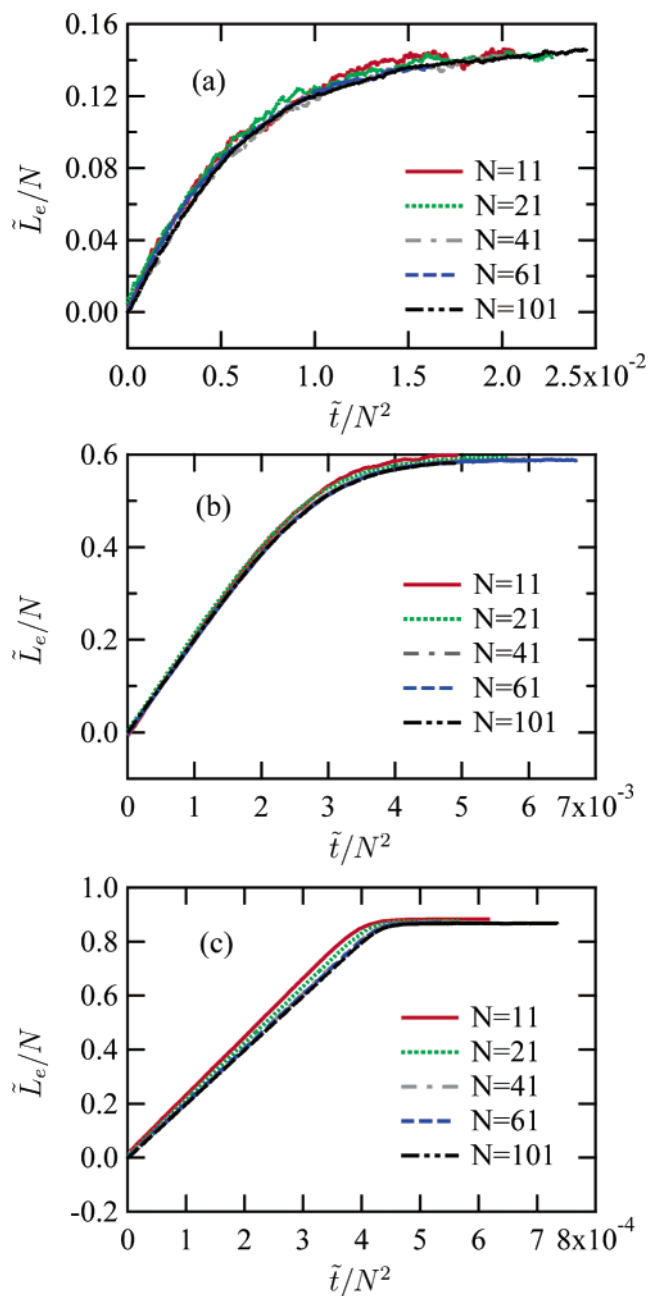


Figure 7. Fractional extension as a function of \tilde{t}/N^2 for wormlike chains of several lengths at Pelet numbers of (a) 1, (b) 10, and (c) 100.

and a clear demarcation exists between the portion of the chain under tension and the remainder of the chain up to the free end. This moving front remains well-defined with time. Such behavior is clearly manifest in Figure 9b at a Pelet number of 100. The behavior of the Rouse chain at the same Pelet number may be inferred by exploiting the linearity of the Rouse model to amplify the scale of the y-axis of Figure 2 by a factor of 100. A subsequent comparison with Figure 9b reveals that tension propagates more gradually in a Rouse chain, as evidenced by its curved tension profiles. The Rouse chain takes longer than the wormlike chain to attain a steady, linear profile. At steady state, the tension in each spring balances the drag on the remainder of the chain up to the free end, and force balance implies that a linear tension profile exists regardless of the spring force law selected. Note that the linearity of the tension profiles at intermediate times indicates that the portion of a wormlike chain under tension at any instant behaves like a shorter, tethered chain at steady state whose length is identical to that of the

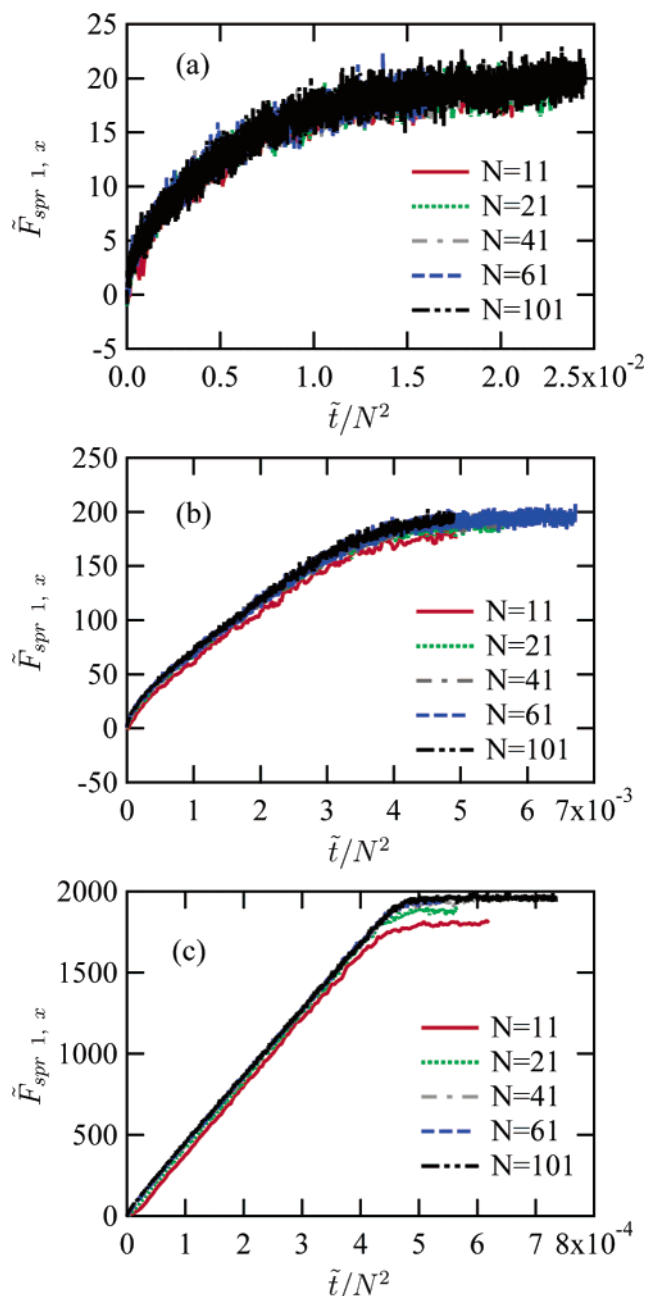


Figure 8. Tension in the first spring as a function of \tilde{t}/N^2 for wormlike chains of several lengths at Pelet numbers of (a) 1, (b) 10, and (c) 100.

tension-bearing segment and that the remainder of the chain not under tension is freely convected by the flow, consequently experiencing no drag.

A further comparison between Rouse and wormlike chains is provided in Figure 10. At early time points, the tension profiles of Rouse and wormlike chains are similar, although the springs of a wormlike chain very close to the tether point become highly stretched even at short times at a high Pelet number. Moreover, tension propagates very quickly in a wormlike chain, and the steady, linear tension profile is evident in a wormlike chain even as the Rouse chain continues to deform.

We next investigate the evolution of the chain length under tension with time. For the sake of definiteness, we associate the number of springs under tension, as illustrated in Figure 11, with the intercept made by the tangent to the tension profile at the tether point on the x -axis. Thus, the symbol n_t denotes

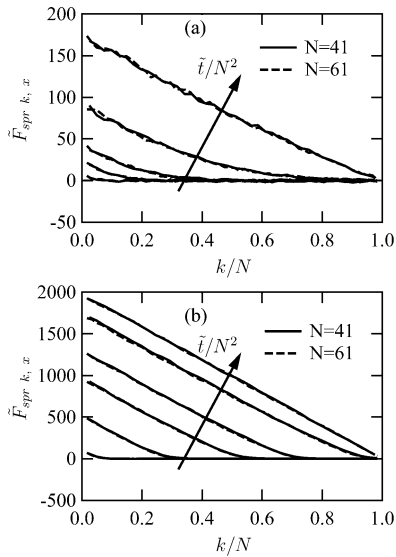


Figure 9. Tension profiles for wormlike chains of 41 and 61 beads as functions of the rescaled spring index k/N at several points in time, compared at equal values of the rescaled time coordinate \tilde{t}/N^2 for both chain sizes at two values of the Peclet number. (a) $Pe = 10$, $\tilde{t}/N^2 = 1.2 \times 10^{-5}$, 1.3×10^{-4} , 4.0×10^{-4} , 1.3×10^{-3} , and 3.4×10^{-3} ; (b) $Pe = 100$, $\tilde{t}/N^2 = 1.2 \times 10^{-5}$, 1.1×10^{-4} , 2.1×10^{-4} , 3.0×10^{-4} , 4.0×10^{-4} , and 5.4×10^{-4} .

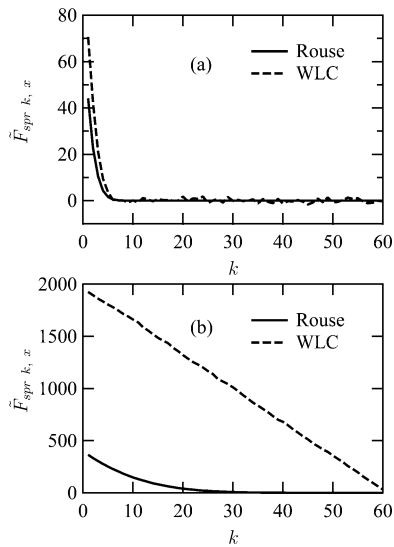


Figure 10. Spring tension as a function of spring index k for 61-bead Rouse and wormlike chains at a Peclet number of 100 at times (a) $\tilde{t} = 0.05$ and (b) $\tilde{t} = 2$.

the number of springs under tension at time t and is determined in a like manner for Rouse and wormlike chains. We allow n_t to be nonintegral.

Figure 12 shows the evolution of n_t with time for Rouse chains of several lengths. Because of the linearity of the Rouse model, n_t is independent of the Peclet number, although the spring tensions themselves grow linearly with the Peclet number. The collapse of data for different chain lengths at early time points reveals that while the deformation of the chain starts at the tether point, the springs closer to the free end continue to be convected by the flow for a longer duration. At longer times, a collapse of data is achieved by a rescaling of the axes, as discussed in section 3.

As a simplified model of tension propagation in a Rouse chain, we consider a semi-infinite chain of beads connected by identical linear springs, lying along the positive x -axis and held fixed at $x = 0$. We further assume that the beads are constrained

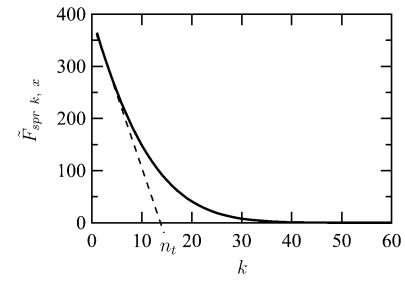


Figure 11. Spring tension as a function of spring index k for a 61-bead Rouse chain at a Peclet number of 100 and at time $\tilde{t} = 2$. The dashed line represents the tangent to the tension profile at the tether point of $k = 1$. The intercept made by the tangent on the x -axis is denoted by n_t , and is interpreted as the number of springs under tension at time \tilde{t} .

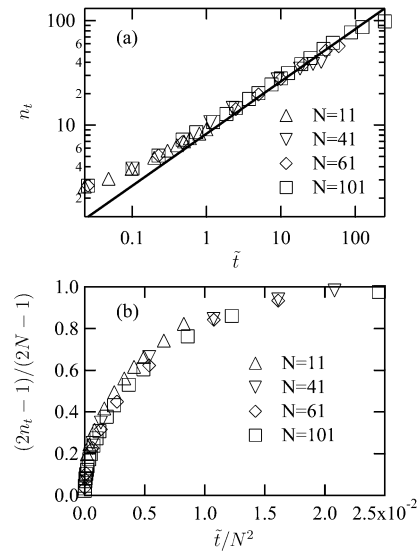


Figure 12. Tension propagation in Rouse chains at a Peclet number of 1. (a) n_t as a function of time for chains of several lengths (open symbols) and that predicted by eq 18 in the continuous limit of a semi-infinite Rouse chain (solid line). (b) Consequent to the rescaling of both axes, a collapse of data for several chain lengths occurs at long time scales.

to move only along the x -axis and that the random thermal forces acting on the beads are negligible. These assumptions are justified upon the imposition of a solvent flow at an unperturbed velocity of v in the positive x -direction at $t = 0$.

Upon going to the continuous limit,³³ we obtain the inhomogeneous diffusion equation

$$\frac{\partial s}{\partial t} = \frac{H}{\zeta} \frac{\partial^2 s}{\partial n^2} + v \quad (14)$$

governing the bead x -displacements $s(n,t)$, where n , denoting the bead index, is now treated as a continuous variable analogous to x . The variable s in eq 14 is analogous to the temperature of a one-dimensional, semi-infinite, heat conducting rod with a constant heat production rate per unit length and with the temperature at $x = 0$ being held fixed at the uniform initial temperature of the rod. Equation 14 may be solved subject to the boundary condition $s(n=0,t) = 0$ and the initial condition $s(n,t=0) = 0$, yielding³⁴

$$s(n,t) = \left(vt + \frac{\zeta v}{2H} n^2 \right) \operatorname{erf} \left(\frac{n}{2\sqrt{Ht/\zeta}} \right) + \sqrt{\frac{\zeta v^2 n^2 t}{\pi H}} \exp \left(-\frac{\zeta n^2}{4Ht} \right) - \frac{\zeta v n^2}{2H} \quad (15)$$

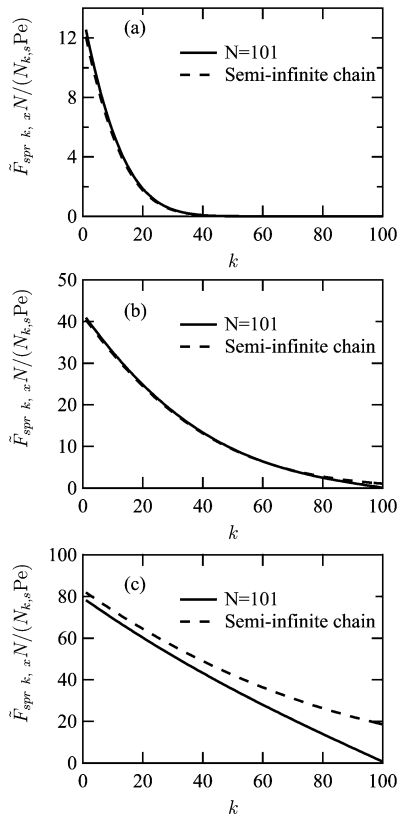


Figure 13. Rescaled spring force $\tilde{F}_{\text{spr } k, x} N / (N_{k, s} \text{Pe})$ as a function of the spring index k for a 101-bead Rouse chain, and that predicted by taking the continuous limit of a semi-infinite Rouse chain at times (a) $\tilde{t} = 2.5$, (b) $\tilde{t} = 25$, and (c) $\tilde{t} = 100$.

The growth of $s(n, t)$, given by eq 15, is suggestive of the diffusive scaling $n_t \sim t^{0.5}$.

Furthermore, eq 15 enables a comparison between the tension profiles obtained from the normal-mode analysis of a finite Rouse chain and those following from the continuous approximation of a semi-infinite chain. The tension in spring n in the continuous limit of the chain is given by the expression $\tilde{F}_{\text{spr } n, x} = \tilde{H} \partial s / \partial n$ in nondimensional form. Hence, use of eq 15 yields the expression

$$\tilde{F}_{\text{spr } n, x} = \frac{\text{Pe} N_{k, s}}{N} \left[n \operatorname{erf} \left(\frac{n}{2\sqrt{\tilde{H}\tilde{t}}} \right) + 2\sqrt{\frac{\tilde{H}\tilde{t}}{\pi}} \exp \left(-\frac{n^2}{4\tilde{H}\tilde{t}} \right) - n \right] \quad (16)$$

for the spring tensions. A comparison between the tension profiles predicted by eq 16 and those obtained for a chain of 101 beads from eqs 5 and 6 is illustrated in Figure 13 at three time points. The tension profiles predicted in the two cases agree when the finite chain is far from steady state. However, as the finite Rouse chain approaches steady state, it is no longer well-approximated by a semi-infinite chain. As expected, the failure of the approximation at later time points is most evident near the free end of the finite chain.

The tangent $T_n(\tilde{t})$ to the instantaneous tension profile $\tilde{F}_{\text{spr } n, x}(\tilde{t})$ from eq 16 at the tethered end $n = 0$ is of the form

$$T_n(\tilde{t}) = \frac{\text{Pe} N_{k, s}}{N} \left(\sqrt{\frac{4\tilde{H}\tilde{t}}{\pi}} - n \right) \quad (17)$$

and consequently

$$n_t = \sqrt{\frac{4\tilde{H}\tilde{t}}{\pi}} \quad (18)$$

Equation 18 establishes that tension propagation in a semi-infinite Rouse chain obeys diffusive scaling.

The existence of a power law dependence of n_t on time for Rouse chains over intermediate time scales is evident from Figure 12a. For chains of lengths $N = 41, 61$, and 101 , the linear region of Figure 12a exhibits the scaling behavior $n_t \sim \tilde{t}^\alpha$ over 2 decades in time, with $\alpha = 0.43, 0.45$, and 0.46 , respectively. Also shown in Figure 12a is the diffusive behavior predicted by eq 18 in the continuous limit of a semi-infinite Rouse chain. We attribute the deviations from diffusive behavior to errors originating from discretization at early time points until the spring closest to the tether point is stretched significantly (beyond its equilibrium root-mean-square length). As steady state is approached, the finiteness of the chain length causes deviations from the behavior expected of a semi-infinite chain.

Finally, we test the hypothesis of the X model proposed by Randall and Doyle⁴ that the length of a tethered DNA chain under tension, denoted here by l_t , grows linearly in time at a rate equal to the velocity of flow, i.e., $l_t = vt$. We hereafter refer to this model as the convective model of tension propagation. While our simulations of wormlike chains provide us with data on the evolution of n_t with time, the deduction of the corresponding chain length under tension requires an estimate of the spring extensions. We obtain such an estimate by first assuming that the lengths of all springs in the tension-bearing segment of the chain at any instant are identical. While this assumption may be justified at a high Peclet number (of the order of 100), we expect it to prove less satisfactory at moderate Peclet numbers of the order of 10.

We are now in a position to estimate the number of springs under tension from the convective model. For this purpose, we employ the large force limit of the Marko–Siggia interpolation formula (eqs 12 and 13, again with the neglect of the tension variation along the chain), in which L_e/L is replaced by the fractional spring extension l_s/Q_0 , in conjunction with the hypothesis that $l_t (= n_l l_s) = vt$. We thereby obtain the following estimate for the number of springs under tension from the convective model:

$$n_t = \frac{vt/Q_0}{1 - (2\text{Pe})^{-1/2}} \quad (19)$$

Figure 14 provides a comparison between the prediction of n_t obtained from the convective model and that obtained from simulation at a Peclet number of 100 for a 61-bead wormlike chain. The convective model predicts a slope of 34.9 for n_t as a function of \tilde{t} at $\text{Pe} = 100$, while a slope of 34.4 with 95% confidence limits of (34.0, 34.8) is obtained from a linear fit to 19 points from simulation. The agreement between the two is impressive, particularly given the assumption of equal spring extensions estimated from the large force limit of the Marko–Siggia law. The corresponding n_t vs \tilde{t} curve for a Rouse chain, shown for comparison, emphasizes the relatively rapid propagation of tension in a wormlike chain.

The transient behavior of the tension in the first spring of the wormlike chain is also illustrated in Figure 14. At a high Peclet number of 100, the tension at the tether point rises linearly from an initial value of zero to its steady value equal to the steady-state drag on the chain, corresponding to $\tilde{F}_{\text{spr } 1, x} = N_{k, s} \text{Pe}$. Steady state is reached once tension propagates up to the free chain end, corresponding to a time of $t \approx Nl_s/v$. The

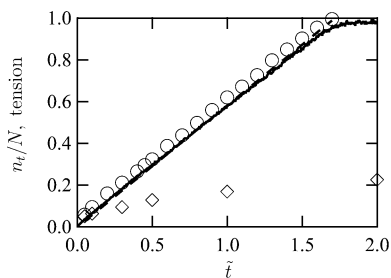


Figure 14. Tension propagation in a 61-bead wormlike chain at a Peclet number of 100. The circles represent n_t/N as a function of \tilde{t} for a wormlike chain and are found to superimpose on the rescaled tension in the first spring $\tilde{F}_{\text{spr } 1, x}/(N_{k,s}\text{Pe})$, scaled to reach a value of unity at steady state (shown by the solid line). Also shown for comparison are the corresponding n_t/N vs \tilde{t} curve for a Rouse chain of identical length (diamonds) and that predicted by the convective model of tension propagation (dashed line).

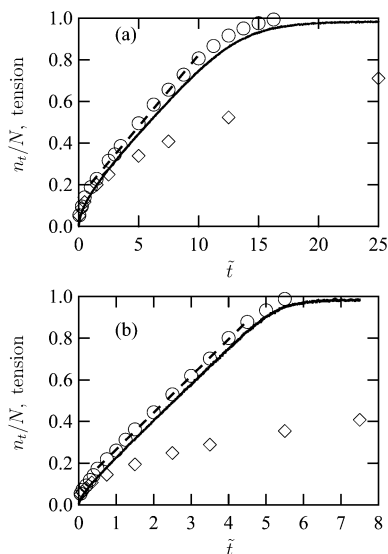


Figure 15. Tension propagation in a 61-bead wormlike chain at Peclet numbers of (a) 10 and (b) 30. The circles represent n_t/N vs \tilde{t} for a wormlike chain. Each dashed line represents the best-fit line passing through the linear region of the corresponding curve for a wormlike chain. Also shown for comparison are the results for a Rouse chain under identical conditions (diamonds). Each solid line is the tension in the first spring rescaled to reach a value of unity at steady state, given by $\tilde{F}_{\text{spr } 1, x}/(N_{k,s}\text{Pe})$.

close accord between n_t/N and $\tilde{F}_{\text{spr } 1, x}/(N_{k,s}\text{Pe})$, where both quantities have been rescaled to attain a value of unity at steady state, reinforces our conclusion that the tension-bearing segment of a wormlike chain instantaneously acts like a shorter, tethered chain at steady state, and the drag it experiences is balanced by the tension at the tether point.

The prediction of the convective model is also tested under moderate conditions of $\text{Pe} = 10$ and $\text{Pe} = 30$. The results are presented in Figure 15, again for a 61-bead chain. At early times, the evolution of n_t in a wormlike chain closely mimics the behavior of a Rouse chain, as expected for stretching in the linear regime. As tension propagates up to the free end of the chain, the springs near the free end, where the drag force is minimum, tend to be weakly stretched in comparison with the springs close to the tether point. Therefore, at moderate flow strengths and at long times, the assumption of equal spring extensions in the portion of the chain under tension and the use of the large force limit of the Marko–Siggia law become increasingly likely to fail. (This feature is also apparent in Figure 6, providing a comparison between the spring extensions at $\text{Pe} = 10$ and $\text{Pe} = 100$.) Consequently, deviations from the

prediction of the convective model are again manifest as steady state is approached. There is, however, an intermediate region during which n_t grows linearly in time, and a comparison with the prediction of the convective model may be made in this region. At $\text{Pe} = 10$, the convective model predicts a slope of 4.18 for n_t vs \tilde{t} . A slope of 4.11 with 95% confidence limits of (3.91, 4.32) is obtained from a linear fit to the 10 points constituting the linear region obtained from simulation. At $\text{Pe} = 30$, the slope of 11.2 predicted by the convective model compares well to the value of 10.6 with 95% confidence limits of (10.4, 10.7) obtained via simulation from a linear fit to 11 points.

The time point at which the crossover occurs from Rouse to convective behavior may be estimated by imposing the equality of the slope $dn_t/d\tilde{t}$ for a semi-infinite Rouse chain, derived from eq 18, and that predicted by the convective model, obtained from eq 19. We thereby obtain the expression

$$\tilde{t}_c = \frac{\tilde{H}}{\pi} \left[\frac{1 - (2\text{Pe})^{-1/2}}{N_{k,s}\text{Pe}/N} \right]^2 \quad (20)$$

for the nondimensional crossover time \tilde{t}_c . A crossover time of $\tilde{t}_c = 1.1$ is predicted by eq 20 at a Peclet number of 10, which is close to the value $\tilde{t}_c = 1.0$ obtained from the simulation data of Figure 15a. At a Peclet number of 30, the predictions of eq 20 and the simulation data of Figure 15b are respectively $\tilde{t}_c = 0.15$ and $\tilde{t}_c = 0.24$. At a Peclet number of 100, eq 20 yields $\tilde{t}_c = 0.015$. However, the prediction of \tilde{t}_c from the simulation data of Figure 14 is hindered by the nonavailability of data points very close to $\tilde{t} = 0$, owing to the discretization error.

Figure 15 reveals that the rescaled tension in the first spring, $\tilde{F}_{\text{spr } 1, x}/(N_{k,s}\text{Pe})$, scaled to reach unity at steady state, closely mirrors the evolution of n_t/N with time at Peclet numbers of 10 and 30. This is consistent with the existence of a similar trend at $\text{Pe} = 100$. However, such a correspondence between n_t and the tension in the first spring is not observed in a Rouse chain, where the rescaled tension in the first spring falls significantly below the evolution of n_t/N vs \tilde{t} curve at intermediate time points before steady state is reached. These observations suggest that the tension-bearing segment of a wormlike chain, but not of a Rouse chain, behaves instantaneously like a shorter, tethered chain of identical length at steady state.

6. Discussion

The present investigation provides an analysis of transient chain stretching in a uniform flow field for a free draining polymer chain modeled as a Rouse chain or as a wormlike chain. The Rouse model is found to provide a satisfactory approximation of a finitely extensible DNA chain at Peclet numbers of the order of 1 or smaller, under which conditions the chain has not been significantly perturbed from the linear, near-equilibrium stretching regime. The dynamic scaling behavior of the Rouse model is readily inferred from the analytical solution of the set of linear Langevin equations governing Rouse dynamics.

As the Peclet number is increased, finite extensibility is found to play a dominant role in determining chain dynamics and in controlling the propagation of tension in the chain. For wormlike chains, as for Rouse chains, the transient fractional extension and spring tensions are found to be universal functions of t/N^2 for different chain lengths N at a fixed value of the Peclet number. The wormlike chain model, unlike the Rouse model, exhibits a nonlinear dependence on the Peclet number, with the chain extension being determined by the cooperative stretching of strongly stretched springs governed by the nonlinear Marko–Siggia force law.

Our results for the time evolution of the chain length under tension indicate a diffusive propagation of tension in Rouse chains. For a wormlike chain, a comparison with the predictions of the convective model of tension propagation is effected by assuming that the springs in the tension-bearing section of the chain have identical extensions, derived from the large force limit of the Marko–Siggia force law. Our results for the tension propagation in a wormlike chain at high Peclet numbers of the order of 100 corroborate the convective model proposed by Randall and Doyle.⁴ At a moderate Peclet number of the order of 10, our results suggest a transition from Rouse behavior at early times to convective tension propagation at later times, and an estimate of the time at which the transition occurs is provided. At still longer times, deviations from convective behavior are observed, possibly because the weak stretching of the springs near the free chain end induces errors in our estimate of the spring lengths. Furthermore, the linearity of the tension profiles and the close agreement between the tension in the first spring and the number of springs under tension at any given point in time suggest that the portion of a wormlike chain under tension acts instantaneously like a steady chain of length identical to that of the tension-bearing section.

A comparison may be made with the scaling arguments of Brochard-Wyart and co-workers,^{20,23} derived for nondraining blobs in a good solvent. Our results for the short time behavior of the chain extension agree with the convective behavior predicted by those authors. This, however, has been interpreted by us as arising from the affine movement of the free chain end, especially at high Peclet numbers. The long time behavior of chain extension is predicted by Brochard-Wyart et al. from the trumpet picture²³ to be an exponential relaxation to steady state with a time constant that is inversely proportional to the flow velocity. In the stem-and-flower regime, Brochard-Wyart's arguments for the long time limit of chain stretching²⁰ imply an exponential relaxation of the chain extension to its steady value with a time constant that is inversely proportional to the square of the flow velocity. These predictions are not reproduced in our results. The linearity of the Rouse model imposes a decoupling of the relaxation times from the solvent velocity. The wormlike chain model predicts a nonlinear dependence of the chain extension on the Peclet number different from that predicted by Brochard-Wyart and co-workers, resulting from the simultaneous stretching of strongly extended wormlike springs. Furthermore, the results of these researchers predict a steady fractional extension proportional to $1 - f^{-1}$, in accord with the behavior of a freely jointed chain acted upon by a drag force of f .³⁵ The steady fractional extension of a strongly stretched wormlike chain is, on the other hand, proportional to $1 - f^{-1/2}$.³⁰ A reformulation of the blob model in a Θ solvent under free draining conditions leads to results in accord with the predictions of the Rouse model.

As previously stated in section 1, hydrodynamic interactions have been neglected in the present work. Experimental studies of DNA dynamics are typically carried out in microchannels whose heights are far exceeded by the chain contour lengths. For example, the experiments of ref 4 employing λ -DNA and T4-DNA having contour lengths of 21 and 70 μm , respectively, were conducted in a microchannel of height 2 μm . Hydrodynamic interactions among chain segments are screened under such conditions, thus partially justifying the free draining assumption.

Our results elucidate the mechanism of transient chain unraveling in uniform flow, relevant to disentanglement processes occurring in post arrays subsequent to a DNA chain—

obstacle collision,^{1,5} in dilute solution capillary electrophoresis,^{7–10} and in flows of polymer solutions.³⁶

Acknowledgment. This material is based upon work supported by the National Science Foundation under Grant No. 0239012 (Career Award).

Appendix

In this section, we present the solution of the Langevin equations, given by eqs 1 and 2, for a Rouse chain. For convenience, we use dimensional notation in the following analysis. The force acting on bead j is given by Hooke's law:

$$\begin{aligned} \mathbf{F}_j &= H(\mathbf{r}_{j+1} - 2\mathbf{r}_j + \mathbf{r}_{j-1}), \quad j = 1, \dots, N-2 \\ &= -H(\mathbf{r}_{N-1} - \mathbf{r}_{N-2}), \quad j = N-1 \end{aligned} \quad (21)$$

Since $\mathbf{r}_0(t) = \mathbf{0} \forall t$, it follows that $\mathbf{F}_1 = H(\mathbf{r}_2 - 2\mathbf{r}_1)$. Therefore, we obtain the equations

$$d\mathbf{r}_j = \left(\mathbf{v} - \frac{H^{N-1}}{\zeta} \sum_{k=1}^{N-1} A_{jk} \mathbf{r}_k \right) dt + \sqrt{\frac{2k_B T}{\zeta}} d\mathbf{W}_j, \quad j = 1, \dots, N-1 \quad (22)$$

where A_{jk} ($j, k = 1, \dots, N-1$) are the matrix elements of the $(N-1) \times (N-1)$ Rouse matrix

$$\mathbf{A} = \begin{bmatrix} 2 & -1 & \cdot & \cdot \\ -1 & 2 & -1 & \cdot \\ \cdot & \cdot & \cdot & \cdot \\ \cdot & \cdot & -1 & 1 \end{bmatrix} \quad (23)$$

\mathbf{A} , being a real, symmetric, positive definite matrix, possesses real, positive eigenvalues and a complete set of orthonormal eigenvectors. Consequently, \mathbf{A} is diagonalized by the similarity transformation $[\mathbf{\Omega}^{-1} \mathbf{A} \mathbf{\Omega}]_{jk} = a_k \delta_{jk}$, where $a_k > 0$ ($k = 1, \dots, N-1$) are the eigenvalues of \mathbf{A} , while $\mathbf{\Omega}$ is the unitary matrix whose columns are the eigenvectors of \mathbf{A} . The unitarity of $\mathbf{\Omega}$ leads to the equality

$$\sum_{j=1}^{N-1} \Omega_{ji} \Omega_{jk} = \delta_{ik}, \quad i, k = 1, \dots, N-1 \quad (24)$$

We now make use of eq 24 to introduce the transformations

$$\mathbf{r}_j = \sum_{k=1}^{N-1} \Omega_{jk} \mathbf{r}'_k \quad (25)$$

$$\mathbf{r}'_k = \sum_{j=1}^{N-1} \Omega_{jk} \mathbf{r}_j \quad (26)$$

By means of the above transformations, eq 22 may be expressed in terms of the variables \mathbf{r}'_k . A subsequent multiplication by Ω_{jm} and a summation over the index j , followed by an application of eq 24 and the similarity transformation, finally yield the set of equations

$$d\mathbf{r}'_m = \left(\sum_{j=1}^{N-1} \Omega_{jm} \mathbf{v} - \frac{H}{\zeta} a_m \mathbf{r}'_m \right) dt + \sqrt{\frac{2k_B T}{\zeta}} d\mathbf{W}'_m, \quad m = 1, \dots, N-1 \quad (27)$$

where we have introduced the independent vector Wiener processes \mathbf{W}'_m via

$$d\mathbf{W}'_m = \sum_{j=1}^{N-1} \Omega_{jm} d\mathbf{W}_j \quad (28)$$

It is readily verified that $\langle d\mathbf{W}'_m(t) \rangle = \mathbf{0}$ and $\langle d\mathbf{W}'_m(t) d\mathbf{W}'_n(t') \rangle = dt \delta_{mn} \delta(t-t') \delta$, with $m, n = 1, \dots, N-1$. The solution of the decoupled, linear stochastic differential equations represented by eq 27 may be effected³⁷ to yield

$$\mathbf{r}'_m(t) = \exp\left(-\frac{H}{\zeta} a_m t\right) \mathbf{r}'_m(0) + \frac{\zeta \mathbf{v}}{H a_m} \left(\sum_{j=1}^{N-1} \Omega_{jm} \right) \left[1 - \exp\left(-\frac{H}{\zeta} a_m t\right) \right] + \sqrt{\frac{2k_B T}{\zeta}} \int_0^t d\mathbf{W}'_m(t') \exp\left(-\frac{H}{\zeta} a_m (t-t')\right) \quad (29)$$

where the stochastic integral on the right-hand side of the above equation is a Gaussian random variable having vanishing mean. An application of eqs 25 and 26 to eq 29 finally yields the expression

$$\mathbf{r}_k(t) = \sum_{m,l=1}^{N-1} \Omega_{km} \exp\left(-\frac{H a_m t}{\zeta}\right) \Omega_{lm} \mathbf{r}_l(0) + \frac{\zeta}{H} \mathbf{v} \sum_{m,j=1}^{N-1} \Omega_{km} \Omega_{jm} \frac{1 - \exp\left(-\frac{H}{\zeta} a_m t\right)}{a_m} + \sqrt{\frac{2k_B T}{\zeta}} \sum_{m=1}^{N-1} \Omega_{km} \int_0^t d\mathbf{W}'_m(t') \exp\left(-\frac{H}{\zeta} a_m (t-t')\right) \quad (30)$$

Since our initial configuration corresponds to an equilibrium Gaussian coil with vanishing mean spring vectors, the mean initial bead positions must also vanish. We now employ eq 30 to derive the mean bead positions at time t :

$$\langle \mathbf{r}_k(t) \rangle = \frac{\zeta}{H} \mathbf{v} \sum_{m,j=1}^{N-1} \Omega_{km} \Omega_{jm} \frac{1 - \exp\left(-\frac{H}{\zeta} a_m t\right)}{a_m} \quad (31)$$

The mean end-to-end distance in the flow direction readily follows from eq 31:

$$L_c = \langle \mathbf{r}_{N-1}(t) \rangle \cdot \hat{\mathbf{x}} = \frac{\zeta}{H} v \sum_{m,j=1}^{N-1} \Omega_{N-1,m} \Omega_{jm} \times \frac{1 - \exp\left(-\frac{H}{\zeta} a_m t\right)}{a_m} \quad (32)$$

The mean spring tension in spring k ($k = 1, \dots, N-1$) in the flow direction is given by the expressions

$$F_{\text{spr } 1, x} = \zeta v \sum_{m,j=1}^{N-1} \Omega_{1m} \Omega_{jm} \frac{1 - \exp\left(-\frac{H}{\zeta} a_m t\right)}{a_m} \quad (33)$$

and

$$F_{\text{spr } k, x} = \zeta v \sum_{m,j=1}^{N-1} (\Omega_{km} - \Omega_{k-1,m}) \Omega_{jm} \frac{1 - \exp\left(-\frac{H}{\zeta} a_m t\right)}{a_m}, \quad k > 1 \quad (34)$$

Equations 32–34 are expressed in the dimensionless notation introduced in section 2 by eqs 4–6.

The eigenvalues and eigenvectors of the Rouse matrix remain to be specified. In our study, we make use of the solution provided by Rzehak and Zimmermann,²⁶ given by eqs 7 and 8.

In the continuous limit of the bead–spring chain, the eigenvalues and eigenvectors are given by the expressions

$$a_m^c = \left[\left(m - \frac{1}{2} \right) \frac{\pi}{N} \right]^2 \quad (35)$$

and

$$\Omega_{jm}^c = \frac{1}{\sqrt{\frac{N}{2} - \frac{1}{4}}} \sin\left(\frac{2m-1}{2N} \pi j\right) \quad (36)$$

with the superscript “c” denoting the continuous approximation. With the exception of the tension in the spring at the free chain end (which becomes negative at very early times), the solution obtained by means of the continuous approximation is found to be indistinguishable from that obtained using the eigenmodes of Rzehak and Zimmermann for a chain of 61 beads, thus reinforcing the scaling of the relaxation times for the slow modes with N^2 for $N \gg 1$.

References and Notes

- (1) Volkmuth, W. D.; Austin, R. H. *Nature (London)* **1992**, *358*, 600–602.
- (2) Randall, G. C.; Doyle, P. S. *Phys. Rev. Lett.* **2004**, *93*, 058102.
- (3) Randall, G. C.; Doyle, P. S. *Macromolecules* **2005**, *38*, 2410–2418.
- (4) Randall, G. C.; Doyle, P. S. *Macromolecules* **2006**, *39*, 7734–7745.
- (5) Doyle, P. S.; Bibette, J.; Bancaud, A.; Viovy, J.-L. *Science* **2002**, *295*, 2237.
- (6) Minc, N.; Bokov, P.; Zeldovich, K. B.; Futterer, C.; Viovy, J.-L.; Dorfman, K. D. *Electrophoresis* **2005**, *26*, 362–375.
- (7) Barron, A. E.; Soane, D. S.; Blanch, H. W. *J. Chromatogr. A* **1993**, *652*, 3–16.
- (8) Barron, A. E.; Blanch, H. W.; Soane, D. S. *Electrophoresis* **1994**, *15*, 597–615.
- (9) Starkweather, M. E.; Muthukumar, M.; Hoagland, D. A. *Macromolecules* **1998**, *31*, 5495–5501.
- (10) Starkweather, M. E.; Hoagland, D. A.; Muthukumar, M. *Macromolecules* **2000**, *33*, 1245–1253.
- (11) Viovy, J.-L. *Rev. Mod. Phys.* **2000**, *72*, 813–872.
- (12) Minc, N.; Viovy, J.-L.; Dorfman, K. D. *Phys. Rev. Lett.* **2005**, *94*, 198105.
- (13) Dorfman, K. D. *Phys. Rev. E* **2006**, *73*, 061922.
- (14) Long, D.; Dobrynin, A. V.; Rubinstein, M.; Ajdari, A. *J. Chem. Phys.* **1998**, *108*, 1234–1244.
- (15) Ferree, S.; Blanch, H. W. *Biophys. J.* **2003**, *85*, 2539–2546.
- (16) Perkins, T. T.; Smith, D. E.; Larson, R. G.; Chu, S. *Science* **1995**, *268*, 83–87.
- (17) Larson, R. G.; Perkins, T. T.; Smith, D. E.; Chu, S. *Phys. Rev. E* **1997**, *55*, 1794–1797.
- (18) Cheon, M.; Chang, I.; Koplik, J.; Banavar, J. R. *Europhys. Lett.* **2002**, *58*, 215–221.
- (19) Brochard-Wyart, F. *Europhys. Lett.* **1993**, *23*, 105–111.
- (20) Brochard-Wyart, F. *Europhys. Lett.* **1995**, *30*, 387–392.
- (21) Rzehak, R.; Kromen, W.; Kawakatsu, T.; Zimmermann, W. *Eur. Phys. J. E* **2000**, *2*, 3–30.
- (22) Rzehak, R.; Kienle, D.; Kawakatsu, T.; Zimmermann, W. *Europhys. Lett.* **1999**, *46*, 821–826.
- (23) Brochard-Wyart, F.; Hervet, H.; Pincus, P. *Europhys. Lett.* **1994**, *26*, 511–516.

- (24) Avramova, K.; Yamakov, V.; Milchev, A. *Macromol. Theory Simul.* **2000**, *9*, 516–522.
- (25) Rzehak, R.; Zimmermann, W. *Europhys. Lett.* **2002**, *59*, 779–785.
- (26) Rzehak, R.; Zimmermann, W. *Phys. Rev. E* **2003**, *68*, 021804.
- (27) Rzehak, R. *Eur. Phys. J. E* **2003**, *11*, 335–348.
- (28) Hallatschek, O.; Frey, E.; Kroy, K. *Phys. Rev. Lett.* **2005**, *94*, 077804.
- (29) Seifert, U.; Wintz, W.; Nelson, P. *Phys. Rev. Lett.* **1996**, *77*, 5389–5392.
- (30) Marko, J. F.; Siggia, E. D. *Macromolecules* **1995**, *28*, 8759–8770.
- (31) Underhill, P. T.; Doyle, P. S. *J. Non-Newtonian Fluid Mech.* **2004**, *122*, 3–31.
- (32) Hsieh, C. C.; Li, L.; Larson, R. G. *J. Non-Newtonian Fluid Mech.* **2003**, *113*, 147–191.
- (33) Doi, M.; Edwards, S. F. *The Theory of Polymer Dynamics*; Clarendon: Oxford, 1986.
- (34) Carslaw, H. S.; Jaeger, J. C. *Conduction of Heat in Solids*, 2nd ed.; Oxford University Press: Oxford, 1959.
- (35) Fixman, M.; Kovac, J. *J. Chem. Phys.* **1973**, *58*, 1564–1568.
- (36) Larson, R. G. *The Structure and Rheology of Complex Fluids*; Oxford University Press: Oxford, 1999.
- (37) Oettinger, H. C. *Stochastic Processes in Polymeric Fluids: Tools and Examples for Developing Simulation Algorithms*; Springer: Berlin, 1996.

MA070050P